Int J Adv Manuf Technol (2018) 94:3841–3852
DOI 10.1007/s00170-017-1078-3

ORIGINAL ARTICLE

An analytical cutting force model for plunge milling of Ti6Al4V considering cutter runout

Kejia Zhuang[1] · **Dahu Zhu**[2] · **Han Ding**[1,3]

Received: 27 February 2017 / Accepted: 12 September 2017 / Published online: 25 September 2017

Abstract As one of the most efficient machining methods, plunge milling has gained more attention as a promising cutting process. This strategy is often used for roughing and semi-roughing processes for the more vibration free than other cutting operations. The motivation of this paper is that the cutting forces in plunge milling differ from that in side milling for the complex cutting condition and tool geometry. In this work, a systematic and analytical cutting force prediction model considering cutter runout for plunge milling is proposed. The detailed analysis of cutting geometry is important for modeling. The precise uncut width is calculated with consideration of the cutting step. In addition, the real-time uncut chip thickness of different inserts is calculated with consideration of the effect of cutter runout. The deduced cutting force model based on the predictive model can be used in various cutting conditions in the plunge milling process. Plunge milling tests with various cutting steps are carried out to verify the proposed model with the quantitative analysis of the results. The results indicate that the simulated results show quite good agreements with the measured cutting forces, which proves the correctness and accuracy of the proposed model.

Keywords Analytical model · Plunge milling · Cutter runout · Cutting force

✉ Dahu Zhu
dhzhu@whut.edu.cn

[1] School of Mechanical and Electronic Engineering, Wuhan University of Technology, Wuhan 430070, China

[2] School of Automotive Engineering, Wuhan University of Technology, Wuhan 430070, China

[3] State Key Laboratory of Digital Manufacturing Equipment and Technology, Huazhong University of Science and Technology, Wuhan 430074, China

Nomenclature

K_t, K_r, K_f	Cutting coefficients in tangential, feed, and radial directions
F_x, F_y, F_z	Cutting force in Cartesian coordinate
Cl_f	Axial relief angles of the tool
V_c	Chip velocity
α_r	Radial rake angle
R	Radius of the tool
$S(\varphi_{ji})$	Real-time dynamic uncut chip
a_s	Nominal cutting step
φ_{ex}	Cutting out angle
φ_{stn}	Changeable cutting angle
ρ	Runout angle
ψ	Lag angle
ε_j	Axial runout amplitude
ϕ_n	Normal shear angle
η_{sh}	Shear flow angle
β_n	Normal friction angle
i	Local helix angle
$\hbar$	Non-equidistant shear band of thickness
T	Instantaneous cutting temperature
λ	The unequal coefficient
C_p	Heat capacity of material
ρ_m	Material density
T_r/T_m	Room/melting temperature
C_1, C_2	The empirical machining constant
β_n	Normal friction angle
χ	Taylor-Quinney coefficient
F_t, F_f, F_r	Cutting force in tangential, feed and radial directions
f_{zj}	Actual feed rate of insert j in normal direction

ψ_r	Cutting edge angle of the tool
V	Cutting velocity
λ_s	Inclination angle
φ_{ji}	Immersion angle of tooth j
f_z	Nominal feed rate of plunge milling
a_e	Nominal cutting width
φ_{st}	Cutting in angle
$t(\varphi_{ji})$	Real-time uncut width thickness
R_j	Actual cutting radius of insert j
λ	Runout offset amplitude
N	Number of cutting teeth
α_n	Normal rake angle
τ_s	Shear flow stress
η_c	The chip flow angle
α_r	Radial rake angle
$\dot{\gamma}$,γ	The shear strain rate, shear strain in the primary shear zone
η_e	Equivalent plane angle
$\dot{\gamma}_m$	Maximum shear strain rate
V_s	Shear velocity
A, B, C, m, n	Yield strength, strength coefficient, strain rate sensitivity coefficient, thermal softening coefficient, and strain hardening exponent of the material, respectively.

1 Introduction

As one of the most important output variables in the metal cutting process, cutting force is one of the key factors affecting the machined surface. The prediction of cutting forces is not only crucial for analyzing and understanding the metal cutting process but also important for optimizing cutting parameters. These models can be used to optimize tool geometry and machining conditions in metal cutting operations. The cutting force model for milling and their theory have been rather well developed and simulated with a numerical algorithm.

During the last decades, there has been significant progress in developing predictive models for cutting operations. The mechanistic model uses cutting force coefficients that are predicted from finite element simulation or calibrated by cutting tests to predict the cutting forces [1]. This kind of method is often used to study the cutting processes for new tool and material design while the high cost of cutting tests limited its application. Kline et al. [2] presented a mechanical cutting force prediction model for peripheral milling. The method put forward by Azeem et al. [3] is the cutting force coefficients obtained from half-slot milling, after which the calibrated coefficients can be applied to a wide range of cutting conditions. Wang et al. [4] studied the average cutting force model and noted that the coefficients can be considered to be constant for the selected tool-workpiece conditions. The results illustrate that the cutting coefficients deriving from the proposed method are independent from the milling parameters selected. Merchant [5] proposed an analytical method based on the orthogonal and oblique cutting theory. Altintas et al. [6] developed an analytical cutting force model for end milling based on the calculation of the chip thickness. Oxley [7] proposed a complex cutting model for low carbon steel based on shear angle, material properties, and other parameters. In the proposed model, the work hardening, strain rate, temperature, and thermal softening of the workpiece are used to evaluate the flow stress of the cutting area. Moufki et al. [8] proposed an analytical thermo-mechanical method, and then they developed the cutting theory and applied it to peripheral milling [9]. Li et al. developed an analytical cutting force model based on the non-equidistant shear zone theory and applied it in end milling operation [10]. The runout effects are investigated with the simulation of cutting force, equivalent stress, and wear characteristics [11, 12]. Fu et al. [13] presented and developed the analytical model considering runout for ball-end milling based on oblique cutting theory.

As one of efficient machining methods, plunge milling operation is more vibration free than other cutting processes, i.e., plane milling, side milling, and end milling. This strategy is often used in roughing and semi-roughing processes [14]. Plunge milling is often used in roughing in molds and dies, also in machining of hard material, such as Inconel 718 for removing excess material rapidly. In plunge milling, the feed direction coincides with the axis direction which highly increases the rigidity of the cutting system. As a result, this machining method has gained more and more attention and research in recent years. Plunge milling operation has received a lot of attention in recent years due to its wide applications in machining of cavities and walls in molds, dies, and aerospace parts. Li et al. [15] developed the cutting force prediction via kinematic integration along the cutting edges, which can facilitate the optimization of tool design and cutting parameters. The intermittent plunge processes are investigated and can be used in vertical walls [16]. The frequency domain model of mechanics and dynamics caused by regenerative chip thickness is proposed by Altintas and Ko [17, 18]. Different cutting conditions (rigid and flexible workpiece) are discussed, and the dynamic chip area is evaluated based on the interaction of the insert main and side cutting edges considering the tool and workpiece geometry [19]. Ren et al. [20] used the plunge strategy for open blisk machining. The new strategy for open blisks reduced the cutting force by 60% and increased the rough machining efficiency more than double. Liang et al. [21] investigated the feed rate scheduling for multi-axis plunge milling of open blisks in order to reduce the machining time. In their study, the material removal rate is scheduled to keep constant and the cutting time reduced by about 23%. Zhuang et al. [22] proposed the plunge cutting force prediction model based on

the precise dynamic uncut chip thickness by considering the cutting step as well as the cutting width. They considered the cutting forces, machine-tool capacity, and stability criteria when improving the cutting parameters in plunge milling. However, the effect of cutter runout existing in the multi-tooth machining process has been ignored in the proposed model. Danis et al. [23] developed the cutting force model in plunge milling of magnesium-rare earth alloys and noted that the tangential force is the preponderant force in plunge milling. In their study, the influences of cutting parameters as well as the edge radius on cutting force are investigated. A wide range of cutting conditions was set to validate the proposed model, and the results showed good agreement between the proposed model and measured results. Rafanelli et al. [24] developed a new method based on the average force model to evaluate the cutting coefficients for plunge milling. The proposed method evaluated the cutting coefficients considering the effect of the radial engagement. Cafieri et al. [25] optimized the plunge milling time via a mixed-integer nonlinear program; the results emphasized the fact that the cutting parameters are very sensitive to the variable cutting forces and machining power constraints.

As one of the most fundamental and important physical parameters, cutting force is the basis for cutting process research. The cutting force prediction models have been widely used for metal cutting by scholars and practitioners. These models are effective when being used in the side cutting processes, such as end milling and flank milling. The contribution of this paper is that an analytical model considering cutter runout for plunge milling based on the classic oblique cutting theory is proposed. In this study, the more accurate engagement geometry reflects the nature of plunge operation by considering the influence of cutter runout and tool angles. The precise real-time cutting width is predicted by the cutting step as well as cutting width. Also, the real-time uncut chip thickness is calculated considering the effect of cutter runout. In addition, the detailed analysis of the cutting geometry for plunge milling with three different conditions is demonstrated in Sect. 2. The classic oblique cutting theory as well as the Johnson-Cook constitutive model is developed for plunge force prediction in Sect. 3. In Sect. 4, the article is followed by a further part of the simulation which verifies the effectiveness and feasibility of the proposed model. Then, the conclusions are given in Sect. 5.

2 Analysis of plunge milling process

2.1 Geometry of plunge milling cutter

The cutting geometry of a classic plunge milling cutter is shown in Fig. 1a which consists of the cutter body and tool inserts from the consideration of economic objective. The method of high-efficiency plunge rough milling is applied in the rough or semi-finishing milling stage. The plunge milling cutter can be used in roughing or semi-roughing, enlarging small holes and making big holes. In plunge milling operation, the cutter inserts have an offset distance from the tool axis and the feed direction is aligned with the spindle axis z, where axes x and y are the horizontal coordinates. Moreover, the main cutting edge is the cutting lip for feed along the axial direction in plunge milling (Fig. 1a) while the main cutting edge is the side edge for feed along the horizontal direction in conventional milling. The systematic cutting force model proposed and validated in this paper is based on the analysis of the precise cutting geometry and cutter runout.

In milling operation, F_t is called tangential cutting force which is going along the direction of the cutting speed, F_f is the one in the direction of feed called feed force, and F_r is the normal cutting force or radial cutting force, as shown in Fig. 1. In order to simplify the analysis, the three predicted orthogonal force components (F_t, F_f, F_r) can be transformed into three orthogonal force components (F_x, F_y, F_z) in Cartesian coordinates. In Fig. 1b, the plunge cutter has an edge angle (ψ_r) and the cutting lip has an offset from the plunge center. The prediction model of the cutting force attracted considerable attention for many years which can be used to guide tool design and cutter production. Figure 1d, e illustrates the oblique cutting theory used in the proposed analytical model. The cutting geometry in plunge milling differs from side milling and end milling. In Fig. 2, the cutting entry zone (ACD) should be taken into account since the cutting step is as great as the radial cutting depth [22]. Figure 2 shows that the plunge milling can be used in roughing, enlarging small holes, and slotting large holes, respectively. Figure 2a illustrates the cutting direction of plunge milling along with the axis of the spindle. There are three different cutting conditions in plunge milling; Fig. 2b, c shows the small cutting width and large cutting width in plunge operation, separately. Figure 2d reflects the slot cutting condition in plunge milling which is a particular case of Fig. 2c.

A detailed analysis of cutting geometry of plunge milling which treats the cutting step and cutting width as equally important factors in modeling has been investigated in this study. Figure 2 gives three cutting conditions in plunge milling with different cutting geometries considering zone ACD. For the jth cutting tooth, φ_{ji} is the immersion angle and $t(\varphi_{ji})$ is the real-time uncut width thickness of the instantaneous cutting position. The detailed explanations of three cutting conditions in plunge milling are given below.

Case 1 Small radial cutting width. As shown in Fig. 2b, the nominal cutting width is smaller than or equal to the tool radius ($a_e \leq R$). The real-time uncut width thickness $t(\varphi_{ji})$ can be given as

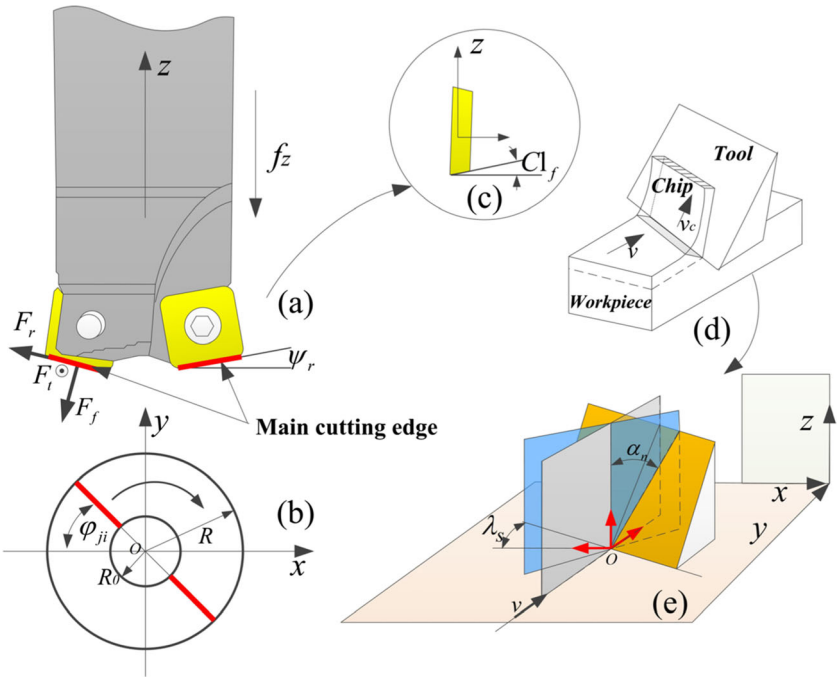

Fig. 1 Geometry of plunge milling tool

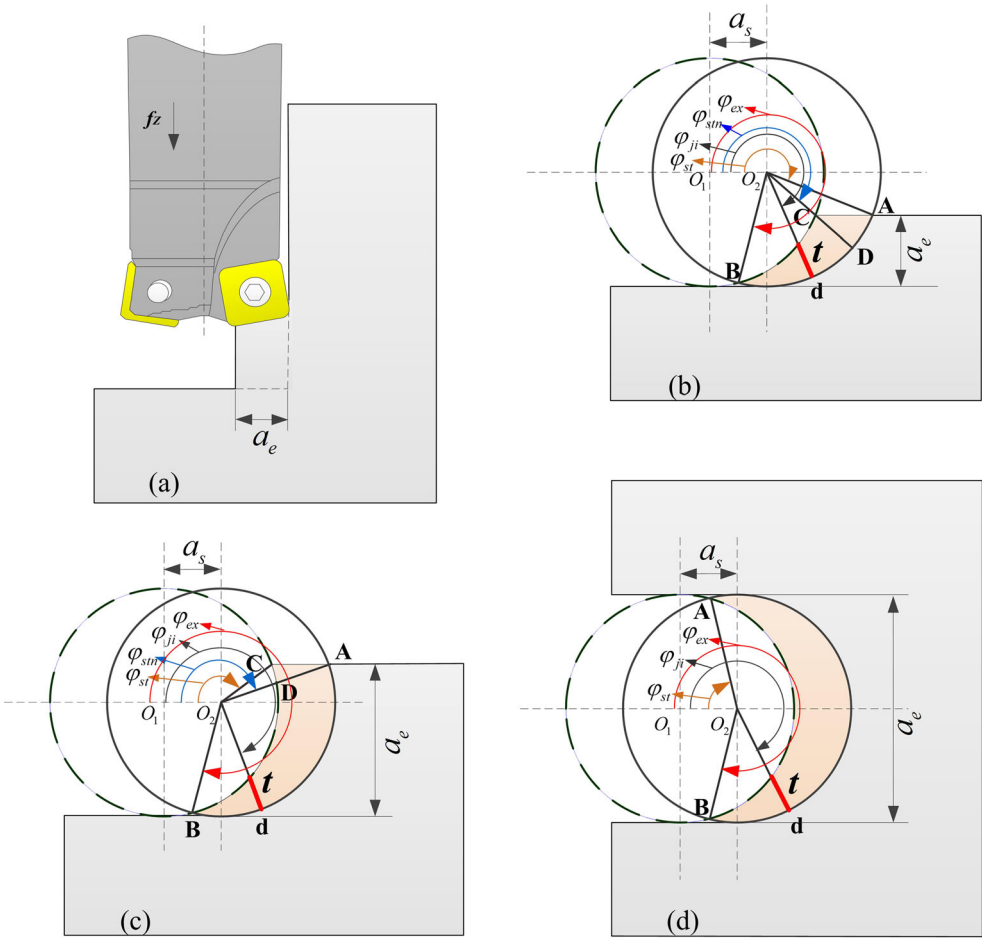

Fig. 2 Cutting geometry of plunge milling with different cutting conditions. **a** Plunge milling process. **b** Small width. **c** Large width. **d** Slot milling

$$t\left(\varphi_{ji}\right)=\begin{cases}0 & \varphi_{ji}<\varphi_{st},\varphi_{ji}>\varphi_{ex}\\ R-\dfrac{a_e-R}{\sin\varphi_{ji}} & \varphi_{st}\le\ \varphi_{ji}\le\ \varphi_{stn}\\ R-\sqrt{R^2-a_s{}^2\cdot\sin^2\varphi_{ji}}-a_s\cdot\cos\varphi_{ji} & \varphi_{stn}\le\ \varphi_{ji}\le\ \varphi_{ex}\end{cases}\quad(1)$$

where

$$\begin{cases}\varphi_{st}=\pi+asin\left(\dfrac{R-a_e}{R}\right)\\ \varphi_{stn}=\pi+atan\left(\dfrac{R-a_e}{\sqrt{2Ra_e-a_e{}^2}-a_s}\right)\\ \varphi_{ex}=\dfrac{3\pi}{2}+atan\left(\dfrac{a_s}{2\mathrm{R}}\right)\end{cases}\quad(2)$$

Case 2 Large radial cutting width. As shown in Fig. 2c, the nominal cutting width is larger than the tool radius ($R < a_e < 2R$).The real-time uncut width thickness $t(\varphi_{ji})$ can be given as

$$t\left(\varphi_{ji}\right)=\begin{cases}0 & \varphi_{ji}<\varphi_{st},\varphi_{ji}>\varphi_{ex}\\ \dfrac{a_e-R}{\sin\varphi_{ji}}-\sqrt{R^2-a_s{}^2\cdot\sin^2\varphi_{ji}}-a_s\cdot\cos\varphi_{ji} & \varphi_{st}\le\ \varphi_{ji}\le\ \varphi_{stn}\\ R-\sqrt{R^2-a_s{}^2\cdot\sin^2\varphi_{ji}}-a_s\cdot\cos\varphi_{ji} & \varphi_{stn}\le\ \varphi_{ji}\le\ \varphi_{ex}\end{cases}\quad(3)$$

where

$$\begin{cases}\varphi_{st}=\pi+atan\left(\dfrac{R-a_e}{\sqrt{2Ra_e-a_e{}^2}-a_s}\right)\\ \varphi_{stn}=\pi+asin\left(\dfrac{R-a_e}{R}\right)\\ \varphi_{ex}=\dfrac{3\pi}{2}+atan\left(\dfrac{a_s}{2\mathrm{R}}\right)\end{cases}\quad(4)$$

Case 3 Slot cutting in plunge milling. As shown in Fig. 2d, the nominal cutting width is equal to the tool diameter ($a_e = 2R$).The real-time uncut width thickness $t(\varphi_{ji})$ can be given as

$$t\left(\varphi_{ji}\right)=\begin{cases}0 & \varphi_{ji}<\varphi_{st},\varphi_{ji}>\varphi_{ex}\\ R-\sqrt{R^2-a_s{}^2\cdot\sin^2\varphi_{ji}}-a_s\cdot\cos\varphi_{ji} & \phi_{st}\le\varphi_{ji}\le\varphi_{ex}\end{cases}\quad(5)$$

where

$$\begin{cases}\varphi_{st}=\dfrac{\pi}{2}-atan\left(\dfrac{a_s}{2\mathrm{R}}\right)\\ \varphi_{ex}=\dfrac{3\pi}{2}+atan\left(\dfrac{a_s}{2\mathrm{R}}\right)\end{cases}\quad(6)$$

For plunge milling, the sum of cutting forces acting on the cutting tooth j at the angular cutting angle φ_{ji} can be expressed as

$$F_{qj}\left(\varphi_{ji}\right)=K_q\cdot S\left(\varphi_{ji}\right)\quad q=t,r,f\quad(7)$$

where $S(\varphi_{ji})$ is the real-time dynamic uncut chip area by cutter tooth j which can be given as

$$S\left(\varphi_{ji}\right)=t\left(\varphi_{ji}\right)f_{zj}\quad(8)$$

The predicted tangential, radial, and feed force given above can be transformed into three orthogonal components in Cartesian coordinates of the cutter axes as follows:

$$\begin{bmatrix}F_{xj}\left(\varphi_{ji}\right)\\ F_{yj}\left(\varphi_{ji}\right)\\ F_{zj}\left(\varphi_{ji}\right)\end{bmatrix}=T\begin{bmatrix}F_{tj}\left(\varphi_{ji}\right)\\ F_{fj}\left(\varphi_{ji}\right)\\ F_{rj}\left(\varphi_{ji}\right)\end{bmatrix}\quad(9)$$

with

$$T=\begin{bmatrix}-\cos\varphi_{ji} & -\sin\psi_r\sin\varphi_{ji} & -\cos\psi_r\sin\varphi_{ji}\\ \sin\varphi_{ji} & -\sin\psi_r\cos\varphi_{ji} & -\cos\psi_r\cos\varphi_{ji}\\ 0 & \cos\psi_r & -\sin\psi_r\end{bmatrix}\quad(10)$$

Then, the integral cutting force on the plunge tool at instantaneous cutting angle can be evaluated

$$F_q(\varphi_i)=\sum_{j=1}^{N}F_{qj}\left(\varphi_{ji}\right)\quad q=x,y,z\quad(11)$$

2.2 Uncut chip thickness with cutter runout

The cutter runout is a common phenomenon in multi-fluted milling operations which cannot be eradicated [2]. The detailed cutter runout and tooth path trajectories are illustrated in Fig. 3. O_1 and O_2 are the centers of axis of the tool and the axis of rotation, and R_j and R_{j-1} are the actual cutting radius in plunge milling with tooth j and $j-1$, respectively. The distance between O_1 and O_2 is characterized as the runout offset amplitude ρ. As shown in Fig. 3, the runout location angle λ is defined to be the angle between the direction O_1O_2 and the negative Y-axis direction. For a cutter with runout, the effective dynamic uncut width of insert j may depend not only on the radius of the cutting insert j but also on the radii of other cutting insets. In plunge milling, the change of cutting radius in the horizontal direction caused by cutter runout is smaller enough to be ignored while its influence on feed direction should be taken into account for the small feed rate. R_j is the actual effective cutting radius of the jth cutting tooth, and this can be obtained by

$$R_j=R+\rho\cos\left(\lambda-\psi-\frac{2(j-1)\pi}{N}\right)\quad(12)$$

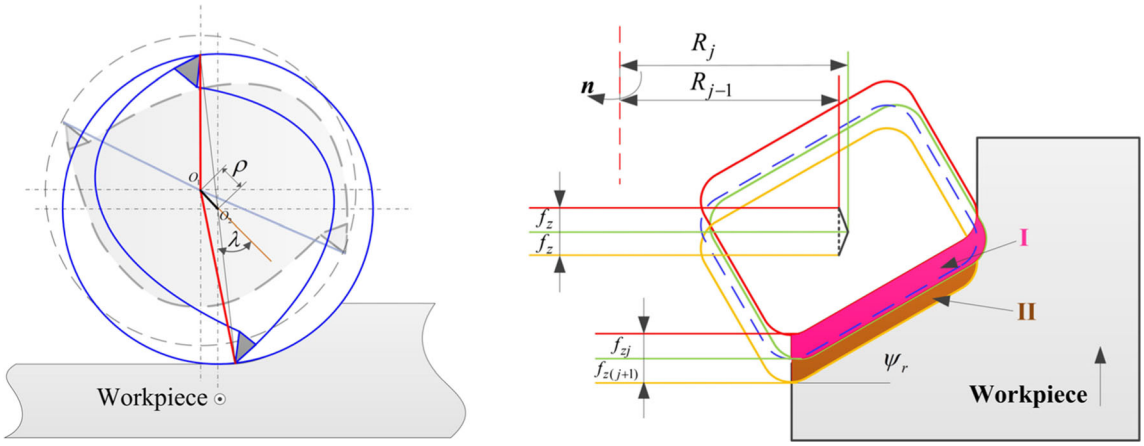

Fig. 3 Cutter runout in plunge milling operation

where ψ is defined as the lag angle and which can be assumed be zero in this study, R is the radius of the cutting tool, and N is the number of the cutting teeth.

In plunge milling, the actual feed in the axis direction differs due to the presence of the entering angle of tool and the cutter runout, as shown in Fig. 3b. Therefore, the instantaneous uncut chip thickness of plunge milling on the jth cutting tooth can be given as

$$f_{zj} = \left(f_z + \varepsilon_j\right)\cdot\cos(\psi_r) \tag{13}$$

where

$$\begin{aligned}\varepsilon_j &= \left(R_j - R_{j-1}\right)\cdot\tan\psi_r \\ &= \rho\left(\cos\left(\lambda - \frac{2(j-1)\pi}{N}\right) - \cos\left(\lambda - \frac{2(j-2)\pi}{N}\right)\right)\cdot\tan\psi_r\end{aligned} \tag{14}$$

3 Cutting force prediction based on oblique cutting model

The equivalent plane method where the cutting process is regarded as a two-dimensional cutting process is often used to analyze the mechanics of oblique cutting as shown in Fig. 4 [10]. In this study, the infinitesimal element of plunge milling can be represented as the oblique cutting process which is analyzed by the equivalent plane method. The cutting force coefficients K_t, K_r, and K_f can be calculated by the following equations by considering the classical oblique cutting model developed by Moufki et al. [9].

$$\begin{cases} K_t = \dfrac{\tau_s}{\cos\lambda_s\sin\phi_n}\cdot\dfrac{\cos\eta_{sh}[\cos\phi_n\cos\lambda_s + \tan\beta_n(\sin\eta_c\sin\lambda_s + \cos\eta_c\sin\phi_n\cos\lambda_s)]}{\cos(\phi_n-\alpha_n)-\tan\beta_n\cos\eta_c\sin(\phi_n-\alpha_n)} \\ K_r = \dfrac{\tau_s}{\cos\lambda_s\sin\phi_n}\cdot\dfrac{\cos\eta_{sh}(-\sin\alpha_n + \tan\beta_n\cos\eta_c\cos\alpha_n)}{\cos(\phi_n-\alpha_n)-\tan\beta_n\cos\eta_c\sin(\phi_n-\alpha_n)} \\ K_f = \dfrac{\tau_s}{\cos\lambda_s\sin\phi_n}\cdot\dfrac{\cos\eta_{sh}[\cos\alpha_n\sin\lambda_s + \tan\beta_n(-\sin\eta_c\sin\lambda_s + \cos\eta_c\sin\alpha_n\sin\lambda_s)]}{\cos(\phi_n-\alpha_n)-\tan\beta_n\cos\eta_c\sin(\phi_n-\alpha_n)} \end{cases} \tag{15}$$

The normal rake angle α_n, normal friction angle β_n, and normal shear angle ϕ_n are determined from the orthogonal cutting approach by using the oblique transformation. According to the matrix transformation and geometric relationship in oblique cutting, essential parameters are summarized in Fig. 4.

The normal rake angle α_n (in the normal plane P_n) is evaluated as [26]

$$\alpha_n = \tan^{-1}(\tan\alpha_r\cos i) \tag{16}$$

where α_r is the radial rake angle and i is the local helix angle and equal to 0.

The equivalent plane angle η_e can be given as follows [5]:

$$\eta_e = \tan^{-1}\left(\frac{\tan\eta_c\cos\eta_{sh} + \sin(\phi_n-\alpha_n)\sin\eta_{sh}}{\cos(\phi_n-\alpha_n)}\right) \tag{17}$$

The shear flow angle η_{sh} is given by [9]:

$$\eta_{sh} = \tan^{-1}\left(\frac{\tan\lambda_s\cos(\phi_n-\alpha_n)-\tan\eta_c\sin\phi_n}{\cos\alpha_n}\right) \tag{18}$$

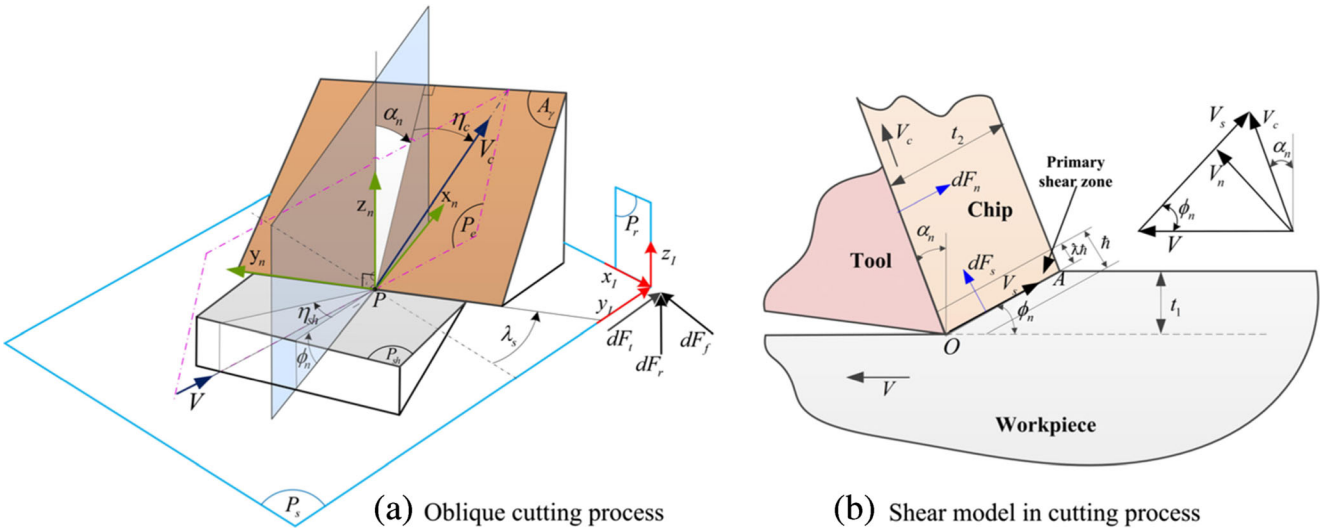

Fig. 4 Oblique cutting process and shear model

The angle between the normal cutting edge line and the direction of the chip flow is defined as the chip flow angle η_c. It can be calculated from the following implicit equation [9].

$$\begin{cases} \tan\lambda_s\tan\beta_n\cos(\phi_n-\alpha_n)\sin(\phi_n-\alpha_n)\cos^2\eta_c-\tan\lambda_s\cos^2(\phi_n-\alpha_n) \\ +\tan\eta_c\sin\phi_n\cos(\phi_n-\alpha_n)+(\cos\alpha_n-\sin\phi_n\sin(\phi_n-\alpha_n))\sin\eta_c\tan\beta_n=0 \end{cases} \tag{19}$$

In Oxley's cutting model, the shear zone is considered as a parallel and equidistant formation. In this study, non-equidistant shear band of thickness $\hbar$ consists of two non-equidistant thickness $(1-\lambda)\hbar$ and $\lambda\hbar$, where $\in[0,1]$. The governing equations for the shear strain rate $\dot{\gamma}$ and the shear strain γ in the primary shear zone can be given in [27].

$$\dot{\gamma}=\begin{cases} \dfrac{\dot{\gamma}_m}{[(1-\lambda)\hbar]^q}[z_e+(1-\lambda)\hbar]^q & z_e\in[-(1-\lambda)\hbar,0] \\ \dfrac{\dot{\gamma}_m}{(\lambda\hbar)^q}(\lambda\hbar-z_e)^q & z_e\in[0,\lambda\hbar] \end{cases} \tag{20}$$

$$\gamma=\begin{cases} \dfrac{\cos\eta_e\dot{\gamma}_m}{V\cos\lambda_s\sin\phi_n(q+1)[(1-\lambda)\hbar]^q}[z_e+(1-\lambda)\hbar]^{q+1} & z_e\in[-(1-\lambda)\hbar,0] \\ -\dfrac{\cos\eta_e\dot{\gamma}_m(\lambda\hbar-z_e)^{q+1}}{V\cos\lambda_s\sin\phi_n(q+1)(\lambda\hbar)^q}+\dfrac{\cos\eta_e\cos\alpha_n}{\sin\phi_n\cos\eta_s\cos(\phi_n-\alpha_n)} & z_e\in[0,\lambda\hbar] \end{cases} \tag{21}$$

The instantaneous cutting temperature T can be evaluated by the heat transfer equation [10].

$$\frac{\partial T}{\partial z_e}=\frac{\cos\eta_e}{\rho_m C_p V\cos\lambda_s\sin\phi_n}\chi\tau\dot{\gamma} \tag{22}$$

The maximum shear strain rate $\dot{\gamma}_m$, the unequal coefficient λ, the chip velocity V_c, and the shear velocity V_s are detailed in Li et al. [27], which are obtained as

$$\dot{\gamma}_m=\frac{(q+1)V_s}{\hbar}=\frac{(q+1)V\cos\lambda_s\cos\alpha_n}{\hbar\cos\eta_{sh}\cos(\phi_n-\alpha_n)} \tag{23}$$

$$\lambda=1-\frac{\cos\eta_{sh}\cos(\phi_n-\alpha_n)(\cos\phi_n\cos\eta_{sh}+\tan\lambda_s\sin\eta_{sh})}{\cos\alpha_n} \tag{24}$$

$$V_c=\frac{V\cos\lambda_s\sin\phi_n}{\cos\eta_c\cos(\phi_n-\alpha_n)} \tag{25}$$

$$V_s=\frac{V\cos\lambda_s\cos\alpha_n}{\cos\eta_s\cos(\phi_n-\alpha_n)} \tag{26}$$

where λ =0.025 mm, q = 3.

Budak et al. [28] analyzed the normal friction angle β_n and presented an analytical dual-zone model of the tool-chip interface. The formula of the normal friction angle β_n and the normal pressure at tool tip P_0 can be derived as follows:

$$\tan\beta_n=\frac{\tau_s}{P_0}\left(1+\xi\left(1-\left(\frac{\tau_s}{\mu_s P_0}\right)^{1/\xi}\right)\right)=\mu_f \tag{27}$$

$$P_0=4\frac{\xi+1}{\xi+2}\frac{\cos^2\beta_n\cos\eta_{sh}}{\sin[2(\phi_n+\beta_n-\alpha_n)]}\tau_s \tag{28}$$

where the exponent for pressure distribution ξ is taken as 3; τ_s is the flow stress of the material, μ_f is the mean friction coefficient, and $\mu_s$is the sliding friction coefficient on the tool-chip interface that can be expressed as $\mu_s = 0.326 + 1.1 \times 10^{-3}V_c$(m/min) [29].

The normal shear angle ϕ_n is essential for estimating the apparent fraction coefficient. It is assumed that the orthogonal shear angle is equal to the normal shear angle in oblique cutting, and a modified Merchant equation given below is used in the present paper.

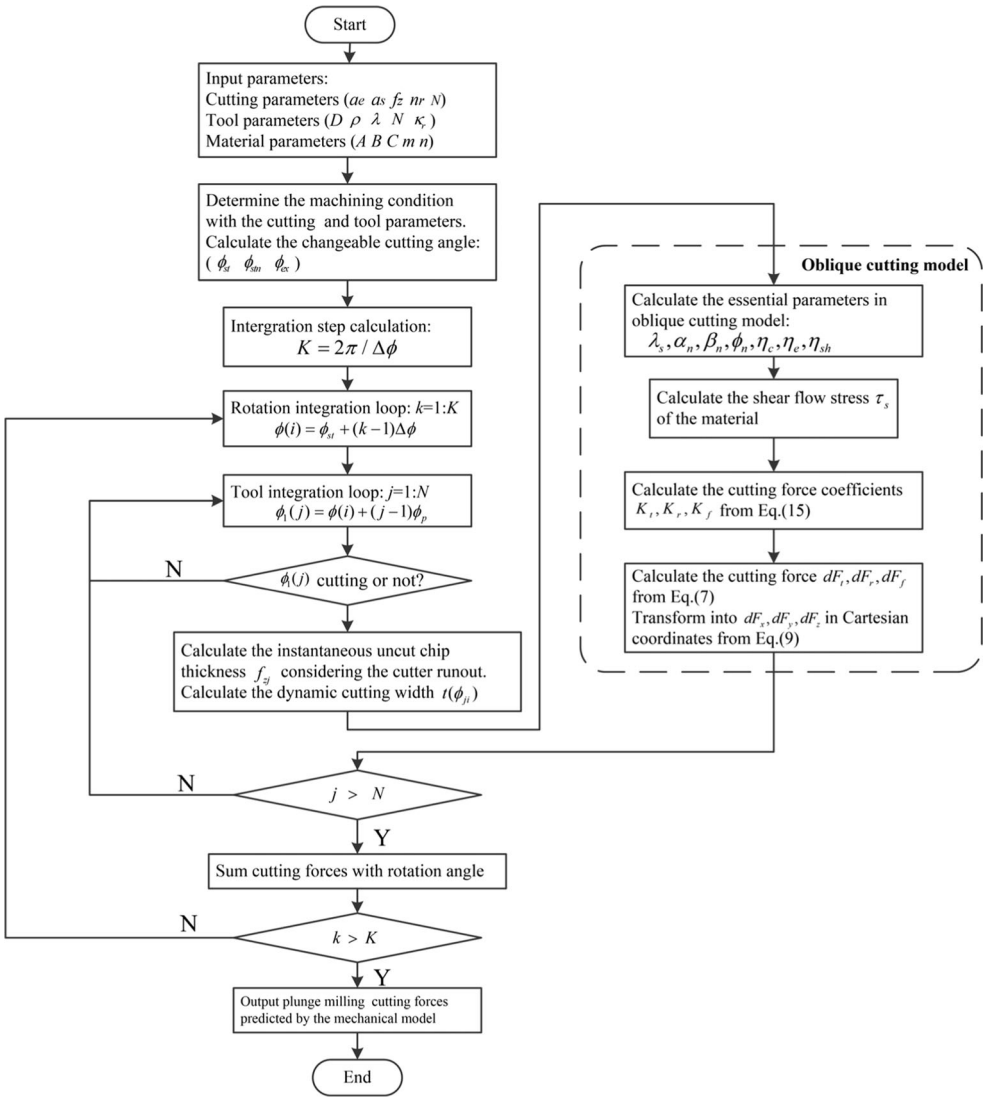

Fig. 5 The flow chart of plunge milling force prediction

$$\phi_n = C_1 - C_2(\beta_n - \alpha_n) \tag{29}$$

where C_1 and C_2 are the empirical machining constants depending on the tool-workpiece material, which are taken as 0.783 and 0.5 in this work, respectively [5].

The constitutive relations are also used to account for the rate of response of materials and their non-linear behavior. Johnson and Cook developed the Johnson-Cook constitutive model which is adopted to evaluate the flow stress, which considers the effects of strain hardening, strain rate, and temperature. In this study, the workpiece is supposed to be

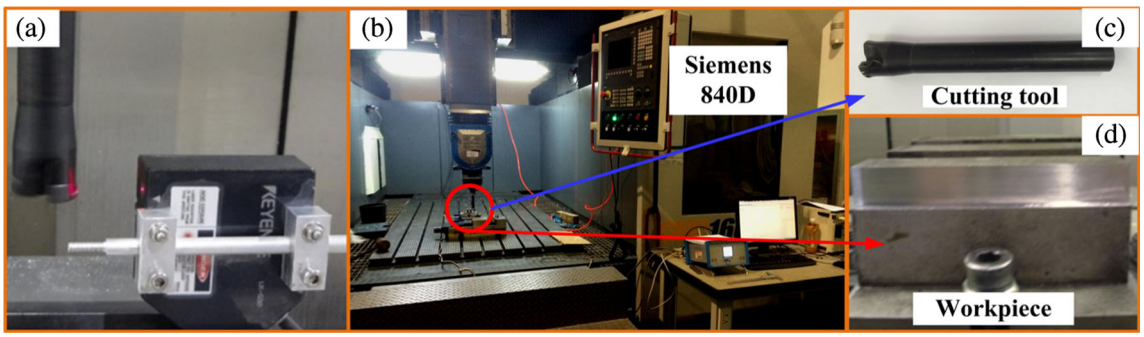

Fig. 6 The experimental setup of plunge milling

Table 1 Characteristics of the Ti6Al4V [13]

ρ (kg/m^3)	C_p (J/kgK)	k_p (W/mK)	χ
4430	526	7	0.85

viscoplastic-rigid and isotropic, and its flow stress τ_s can be given as

$$\tau_s = \frac{1}{\sqrt{3}}\left(A + B\left(\frac{\gamma}{\sqrt{3}}\right)^n\right)\left(1 + C\ln\left(\frac{\dot{\gamma}}{\dot{\gamma}_0}\right)\right)\left(1-\left(\frac{T-T_r}{T_m-T_r}\right)^m\right) \quad (30)$$

With the proposed model illustrated above, the corresponding computer programs in Matlab are developed to implement on the analysis of the cutting force model. In this paper, the uncut chip thickness and cutting velocity are modified according to the given equations with consideration of the cutter runout. The detailed algorithm used to predict the cutting force is proposed in this study, and the flow chart of the procedure is shown in Fig. 5.

4 Experimental validation and analysis

4.1 Experimental conditions

In this section, a series of cutting tests are accomplished to validate the proposed analytical cutting force prediction model in plunge milling operation. As shown in Fig. 6, the experiments of plunge milling are performed in a five-axis milling center with a Siemens 840D numerical control system. As shown in Fig. 6a, before the cutting tests, the laser sensor is used to obtain the runout offset with its orientation angle of the plunge tool. In the cutting tests, a Kistler 9257A dynamometer with an amplifier is used to measure the three-direction cutting forces in the Cartesian coordinate system. Figure 6b shows the experimental setup of the plunge milling operation. Figure 6c, d illustrates the geometry of the cutting tool and workpiece, respectively. The data signals acquired by the sensors are collected by an NI acquisition instrument which is connected to a computer.

As shown in Fig. 5, the cutting parameters, material parameters, and tool parameters in plunge milling are the input variables in the proposed model. The workpiece used in the cutting tests is Ti6Al4V with the size of a rectangle block, as shown in Fig. 6d. This kind of material is often used in aircraft turbine engines. Table 1 lists the properties of this kind of material, and the Johnson-Cook parameters of Ti6Al4V are given in Table 2. A 32-mm plunge milling tool holder with two inserts are used in plunge milling processes under dry cutting, and the cutting tool used in the cutting tests is shown in Fig. 6c. The cutting edge angle ψ_r is 10°, and the cutter inserts can be replaced by new ones out of economic consideration. There are three types of cutting in plunge milling operations, i.e., small width, large width, and slot. In this section, a series of plunge experiments are performed to validate the proposed model. The typical cutting conditions from the cutting tests are given in Table 3 with the cutter runout parameters measured by a laser sensor.

Table 2 Johnson-Cook parameters of Ti6Al4V [13]

A (MPa)	B (MPa)	C (MPa)	n	m	(γ_0/s)	T_m (°C)	T_r (°C)
862.5	331.2	0.012	0.34	0.8	1	1993	20

4.2 Results comparisons

The cutting force simulation with the proposed model for plunge milling operation is carried out. Figure 7 proposes the theoretical prediction cutting forces under the given cutting conditions (Table 3), which are in good agreement with the measurement ones on the waveform, amplitude, and phase. From the comparison results, it can be seen that the cutter runout phenomenon existed in the two-fluted plunge milling operation. The cutter runout parameters can be calculated with the measured data from the laser sensor, and the runout parameters are given in Table 3. The measured cutting forces show varying amplitudes under different cutting inserts, and the cutting forces predicted carried the same rule by considering the cutter runout effect in Sect. 2.2.

For further comparison of the predictive and experimental results, quantitative and detailed analysis based on the data is given. First, the average cutting forces obtained from the predicted by the proposed analytical model and experiments are compared; the errors of the average value of forces in three directions are calculated and given in Table 4. The values in the list represent that the average absolute forces are obtained from the cut-in rotation section in one revolution of the cutter for reducing the error. In the present work, it can be noted that the average errors of three directions are smaller than 15%, which shows that the proposed model performs well with the measured ones. In order to compare the trends of predictive and experimental results, the correlation between two results are used and the correlation coefficients are given in Table 4 [29]. The average correlation coefficient is 0.9584 which shows that the data are highly correlated. The predicted and measured plunge forces are in good quantitative agreement, which indicates the correctness of the proposed model in Sect. 3 with consideration of the cutter runout.

5 Conclusions

In this work, an analytical cutting force prediction model considering the cutter runout phenomenon for plunge milling is proposed. The developed model is based on the fundamental

Table 3 Cutting parameters under different cutting conditions

No.	Type	D	Ω	a_e	a_s	f_z	ρ	λ
1	Small	32	1000 rpm	5 mm	5 mm	0.05 mm/tooth	12 μm	27°
2	Small	32	1000 rpm	5 mm	5 mm	0.10 mm/tooth		
3	Small	32	1000 rpm	12 mm	4 mm	0.08 mm/tooth		
4	Large	32	1000 rpm	20 mm	6 mm	0.05 mm/tooth		
5	Large	32	1000 rpm	24 mm	5 mm	0.05 mm/tooth		
6	Slot	32	1000 rpm	32 mm	5 mm	0.05 mm/tooth		

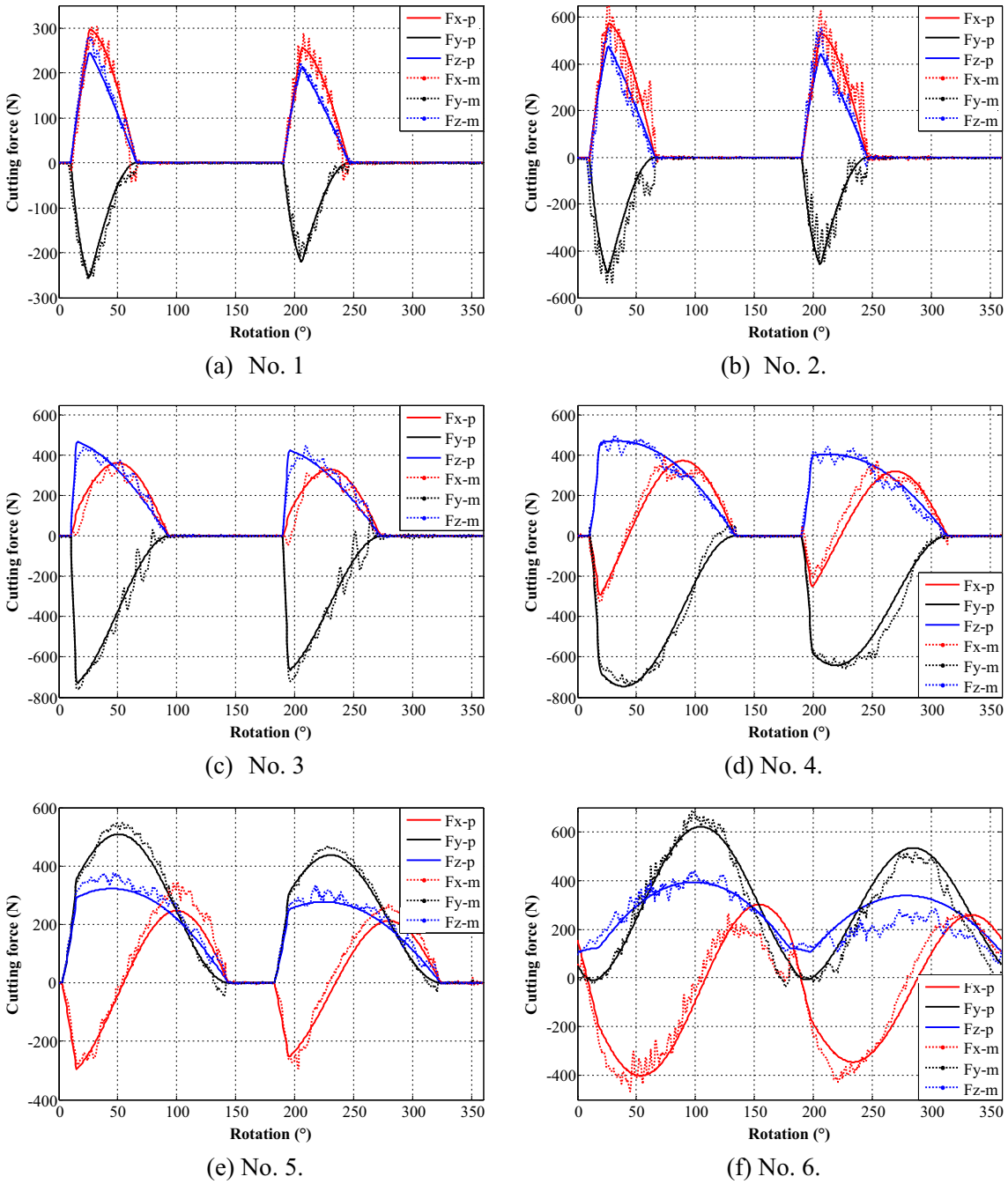

Fig. 7 The predicted and measured cutting forces with the cutting parameters shown in Table 3

Table 4 Average cutting forces of measured and predicted by proposed model and their errors

No.	Predicted			Measured			Error					
	Average			Average			Average(%)			Correlation coefficient		
	Fx	Fy	Fz	Fx	Fy	Fz	Fx	Fy	Fz	Fx	Fy	Fz
1	172.0	110.8	134.4	161.5	104.2	123.7	6.1	6.0	8.0	0.9565	0.9705	0.9872
2	341.4	238.8	250.3	323.1	208.4	247.4	5.4	12.8	2.5	0.9071	0.8963	0.9532
3	205.4	410.4	288.6	201.1	400.2	301.1	2.1	2.5	−4.3	0.9677	0.9857	0.9799
4	191.9	340.2	271.3	218.4	319.9	262.2	12.1	5.9	3.4	0.9457	0.9845	0.9595
5	168.8	287.1	227.1	145.3	275.6	207.3	13.9	4.0	8.8	0.9941	0.9967	0.9900
6	208.1	276.9	236.9	221.9	305.8	265.0	6.6	10.4	11.8	0.9493	0.9786	0.8497

metal cutting principles and precise uncut chip thickness prediction in plunge milling. The cutting step as well as cutting width are used to predict the real-time dynamic cutting width and uncut chip thickness in plunge milling process. The forces predicted by the proposed model closely match the measured ones for the whole cutting conditions in plunge milling operation. The following conclusions can be given from this study:

1. An analytical cutting force prediction model considering the workpiece material constitutive law, cutting parameters, tool geometry, and cutting conditions is proposed and developed for plunge milling operation. In the new prediction model, the Johnson-Cook constitutive law is used to estimate the shear flow stress which is used to calculate the cutting coefficients used for plunge milling operation.
2. Plunge milling differs from other cutting processes for the feed along the axis of the spindle. The cutting step as well as the cutting width are used to predict the real-time dynamic uncut chip in three cutting conditions. The effects of cutter runout parameters on the uncut chip thickness by the tool edge angle are analyzed with the precise cutting geometry.
3. The quantitative and detailed analysis of the experimental and predictive results is given in this investigation. The qualitative analysis shows that the predicted cutting forces match the measured ones well, which proves the effectiveness and feasibility of the proposed model.

In this study, the proposed model and its theory are described in detail and designed for accuracy control of plunge milling. The algorithm developed by the proposed model is proved to be correct and feasible by the comparison of measured and predicted results. The influences of cutting parameters on the cutting forces in plunge milling should be studied and analyzed in future study.

Acknowledgements This work is partially supported by the National Natural Science Foundation of China (51705385, 51675394, 51605353), the Hubei Province Natural Science Foundation of China (2015CFB698), the State Key Laboratory of Digital Manufacturing Equipment and Technology (DMETKF2017019), and the Fundamental Research Funds for the Central Universities (WUT: 2017-IVA-016, 2017II27GX).

References

1. Engin S, Altintas Y (2001) Mechanics and dynamics of general milling cutters.: part I: helical end mills. Int J Mach Tools Manuf 41(15):2195–2212
2. Kline WA, DeVor R (1983) The effect of runout on cutting geometry and forces in end milling. Int J Mach Tool Des Res 23(2):123–140
3. Azeem A, Feng H-Y, Wang L (2004) Simplified and efficient calibration of a mechanistic cutting force model for ball-end milling. Int J Mach Tools Manuf 44(2):291–298
4. Wang M, Gao L, Zheng Y (2014) An examination of the fundamental mechanics of cutting force coefficients. Int J Mach Tools Manuf 78:1–7
5. Merchant ME (1945) Mechanics of the metal cutting process. I. Orthogonal cutting and a type 2 chip. J Appl Phys 16(5):267–275
6. Altintas Y, Spence A, Tlusty J (1991) End milling force algorithms for CAD systems. CIRP Ann Manuf Technol 40(1):31–34
7. Oxley PLB, Young H (1989) The mechanics of machining: an analytical approach to assessing machinability. Ellis Horwood Publisher:136–182
8. Moufki A, Dudzinski D, Molinari A, Rausch M (2000) Thermoviscoplastic modelling of oblique cutting: forces and chip flow predictions. Int J Mech Sci 42(6):1205–1232
9. Moufki A, Dudzinski D, Le Coz G (2015) Prediction of cutting forces from an analytical model of oblique cutting, application to peripheral milling of Ti-6Al-4V alloy. Int J Adv Manuf Technol 81(1–4):615–626
10. Li B, Hu Y, Wang X, Li C, Li X (2011) An analytical model of oblique cutting with application to end milling. Mach Sci Technol 15(4):453–484
11. Yang K, Liang Y-c, Zheng K-n, Q-s B, W-q C (2011) Tool edge radius effect on cutting temperature in micro-end-milling process. Int J Adv Manuf Technol 52(9):905–912. https://doi.org/10.1007/s00170-010-2795-z
12. Bai Q, Yang K, Liang Y, Yang C, Wang B (2009) Tool runout effects on wear and mechanics behavior in microend milling. J Vac Sci Technol B: Microelectronics Nanometer Struct Process Meas Phenom 27(3):1566–1572
13. Fu Z, Yang W, Wang X, Leopold J (2016) An analytical force model for ball-end milling based on a predictive machining theory

considering cutter runout. Int J Adv Manuf Technol 84(9–12): 2449–2460
14. Zhuang K, Zhang X, Ding H (2013) Cutting force prediction of plunge milling based on precise cutting geometry. In: Intelligent Robotics and Applications. Springer, pp 592–601
15. Li Y, Liang S, Petrof R, Seth B (2000) Force modelling for cylindrical plunge cutting. Int J Adv Manuf Technol 16(12):863–870
16. Wakaoka S, Yamane Y, Sekiya K, Narutaki N (2002) High-speed and high-accuracy plunge cutting for vertical walls. J Mater Process Technol 127(2):246–250
17. Altintas Y, Ko J (2006) Chatter stability of plunge milling. CIRP Ann Manuf Technol 55(1):361–364
18. Ko JH, Altintas Y (2007) Dynamics and stability of plunge milling operations. J Manuf Sci Eng 129(1):32–40
19. Damir A, Ng E-G, Elbestawi M (2011) Force prediction and stability analysis of plunge milling of systems with rigid and flexible workpiece. Int J Adv Manuf Technol 54(9–12):853–877
20. Ren J, Yao C, Zhang D, Xue Y, Liang Y (2009) Research on tool path planning method of four-axis high-efficiency slot plunge milling for open blisk. Int J Adv Manuf Technol 45(1):101–109
21. Liang Y, Ren J, Zhang D, Li X, Zhou J (2015) Mechanics-based feedrate scheduling for multi-axis plunge milling. Int J Adv Manuf Technol 79(1–4):123–133
22. Zhuang K, Zhang X, Zhang D, Ding H (2013) On cutting parameters selection for plunge milling of heat-resistant-super-alloys based on precise cutting geometry. J Mater Process Technol 213(8):1378–1386
23. Danis I, Wojtowicz N, Monies F, Lagarrigue P (2014) Influence of dry plunge-milling conditions on surface integrity of magnesium alloys. Int J Mechatronics Manuf Syst 5 7(2–3):141–156
24. Rafanelli F, Campatelli G, Scippa A (2015) Effects of cutting conditions on forces and force coefficients in plunge milling operations. Adv Mech Eng 7(6):1687814015589547
25. Cafieri S, Monies F, Mongeau M, Bes C (2016) Plunge milling time optimization via mixed-integer nonlinear programming. Comput Ind Eng 98:434–445
26. Armarego EJA, Brown RH (1969) The machining of metals
27. Li B, Wang X, Hu Y, Li C (2011) Analytical prediction of cutting forces in orthogonal cutting using unequal division shear-zone model. Int J Adv Manuf Technol 54(5–8):431–443
28. Budak E, Ozlu E (2008) Development of a thermomechanical cutting process model for machining process simulations. CIRP Ann Manuf Technol 57(1):97–100
29. Hollander M, Wolfe DA, Chicken E (2013) Nonparametric statistical methods. John Wiley & Sons